Journal of Controlled Release 378 (2025) 145–152

Contents lists available at ScienceDirect

Journal of Controlled Release

journal homepage: www.elsevier.com/locate/jconrel

Modular functionalization of cellular nanodiscs enables targeted delivery of chemotherapeutics into tumors

Ilkoo Noh [a,1,2], Zhongyuan Guo [a,2], Rui Wang [a], Audrey T. Zhu [a], Nishta Krishnan [a], Animesh Mohapatra [a], Weiwei Gao [a], Ronnie H. Fang [a,b,*], Liangfang Zhang [a,*]

[a] Aiiso Yufeng Li Family Department of Chemical and Nano Engineering, Shu and K.C. Chien and Peter Farrell Collaboratory, University of California San Diego, La Jolla, CA 92093, USA

[b] Division of Host-Microbe Systems and Therapeutics, Department of Pediatrics, University of California San Diego, La Jolla, CA 92093, USA

ARTICLE INFO

Keywords:
Cellular nanoparticle
SpyCatcher/SpyTag
Modular nanoparticle
Targeted delivery
Chemotherapy

ABSTRACT

The effective delivery of chemotherapeutic drugs to tumor sites is critical for cancer treatment and remains a significant challenge. The advent of nanomedicine has provided additional avenues for altering the in vivo distribution of drug payloads and increasing tumor localization. More recently, cell-derived nanoparticles, with their biocompatibility and unique biointerfacing properties, have demonstrated considerable utility for drug delivery applications. Here, we demonstrate that cell membrane-derived nanodiscs can be employed for tumor-targeted delivery. To bestow active targeting capabilities to the cellular nanodiscs, we utilize a modular functionalization strategy based on the SpyCatcher system. This enables the nanodiscs to be covalently modified with any targeting ligand labeled with a short SpyTag peptide sequence. As a proof-of-concept, a model chemotherapeutic doxorubicin is loaded into nanodiscs functionalized with an affibody targeting epidermal growth factor receptor. The resulting nanoformulation demonstrates strong tumor targeting both in vitro and in vivo, and it is able to significantly inhibit tumor growth in a murine breast cancer model.

1. Introduction

Recognized as the second leading cause of death worldwide, cancer presents a significant public health challenge [1,2]. While newer treatment modalities such as targeted therapies, immunotherapies, and various combination approaches have proven to be effective against certain cancers [3–5], chemotherapy remains a common frontline treatment [6]. In general, chemotherapeutics function by targeting rapidly dividing cancer cells, whether by affecting cell division, damaging DNA, or inducing apoptosis [7]. Despite their effectiveness, such therapies are oftentimes encumbered by off-target toxicity, as their mechanisms of action are not specific to cancer cells [8]. This considerably limits amount of drug that can be administered to patients, providing an avenue for tumors to develop drug resistance mechanisms that ultimately result in recurrence [9]. For chemotherapies, their dose-limiting toxicities are largely an issue of nonspecific delivery, as systemic administration results in the unwanted exposure of healthy tissue to cytotoxic drugs [10,11]. Further, it is well-known that many potent cancer therapeutics suffer from low bioavailability due to their hydrophobic nature [12]. As such, drug delivery strategies that can localize large amounts of payload more specifically into tumor sites have been highly sought after.

The emergence of nanotechnology has helped to transform the field of drug delivery, enabling more precise control over the in vivo distribution of pharmaceuticals [13]. This is facilitated by the unique properties of nanoparticles, including their small size, large surface area-to-volume ratio, ability to encapsulate various drug payloads, and amenability to surface modification [14]. Currently, several nanodrugs have been approved for clinical use against cancers, including Doxil, a doxorubicin (DOX)-loaded liposome, and Abraxane, a paclitaxel-bound albumin nanoparticle [15,16]. In general, first generation nanomedicine platforms have relied on passive targeting mechanisms such as the

* Corresponding authors at: Aiiso Yufeng Li Family Department of Chemical and Nano Engineering, Shu and K.C. Chien and Peter Farrell Collaboratory, University of California San Diego, La Jolla, CA 92093, USA.

E-mail addresses: rhfang@ucsd.edu (R.H. Fang), zhang@ucsd.edu (L. Zhang).

[1] Present address: Department of Medical Biotechnology, Division of Biomedical Convergence, Kangwon National University, Chuncheon 24,341, Republic of Korea.

[2] These authors contributed equally to this work.

https://doi.org/10.1016/j.jconrel.2024.12.004
Received 22 July 2024; Received in revised form 27 November 2024; Accepted 3 December 2024
Available online 12 December 2024

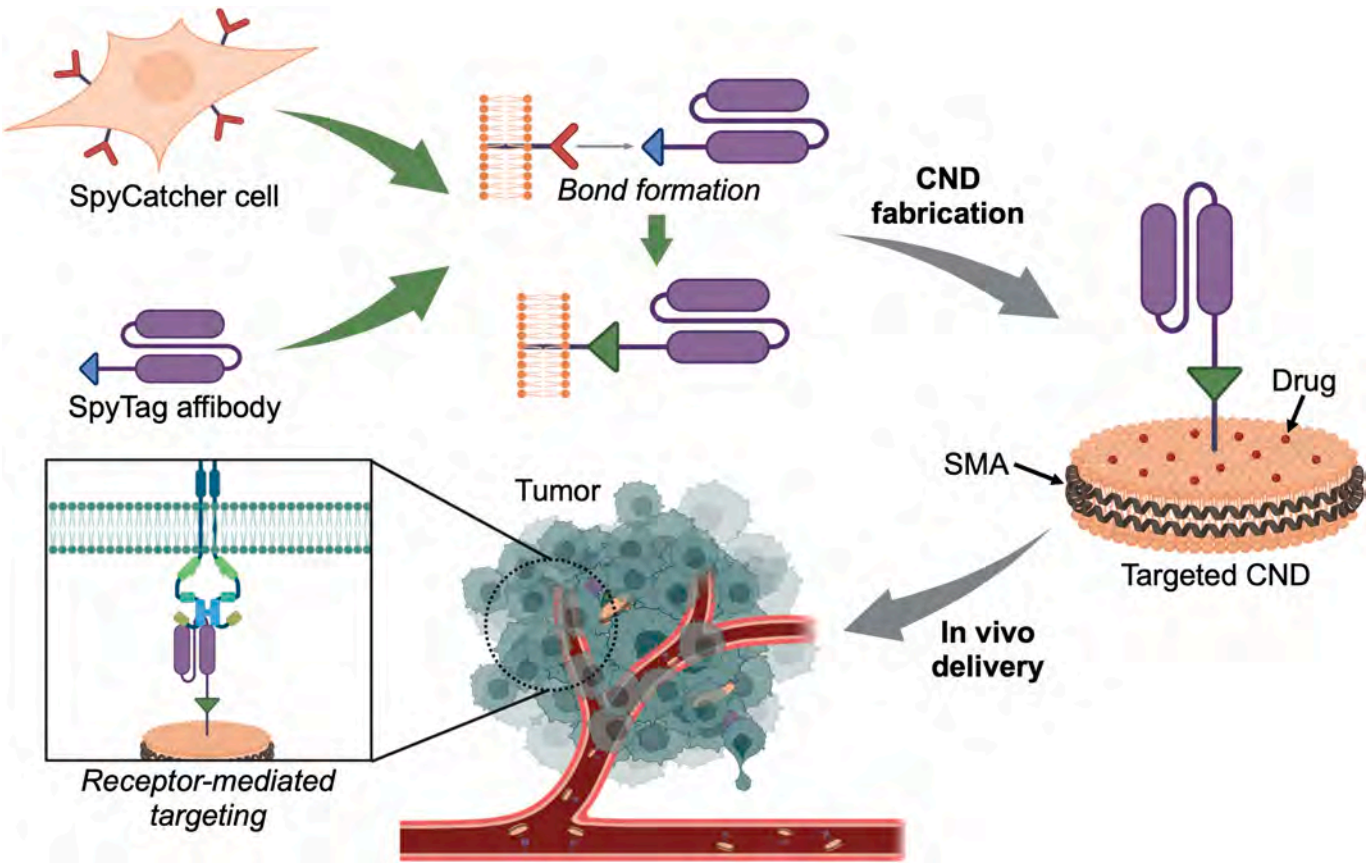

Fig. 1. Modular functionalization of cellular nanodiscs (CNDs) for targeted tumor delivery. Source cells are modified to express SpyCatcher on their surface, which enables their membrane to be covalently functionalized with a targeting ligand fused to the SpyTag peptide. The modified membrane from these cells can then be used to fabricate drug-loaded CNDs with the help of the styrene-maleic acid (SMA) copolymer. The resulting nanoformulation can subsequently target tumors positive for the cognate receptor of the affibody. Created with Biorender.

enhanced permeability and retention effect to accumulate at the tumor site [17]. To further improve efficiency, later generation nanodrugs have employed active targeting, which can be achieved through the use of ligands such as antibodies, peptides, aptamers, and nutrient mimetics [18–20]. More recently, biomimetic nanoparticles have been gaining attention due to their ability to recapitulate functions commonly found in nature [21]. Among these, cell membrane-coated nanoparticles (CNPs), composed of a nanosized core and a cell membrane shell, have emerged as a promising platform [22–24]. As a result of their cell-mimicking properties, CNPs are capable of immune evasion, inflammation targeting, and cancer homing, making them valuable tools for tumor targeting [25,26].

Building upon the CNP concept, researchers have demonstrated that it is possible to fabricate cellular nanodiscs (CNDs) composed of cell membrane stabilized by an amphiphilic polymer [27]. CNDs, characterized by their extremely small size and disc-shaped morphology, have emerged as a promising nanoplatform for various biomedical applications. For example, they can excel at antigen delivery and have been employed to elicit potent antitumor and antibacterial immunity [27,28]. CNDs have also been utilized to successfully neutralize various bacterial toxins both in vitro and in vivo [29,30]. Here, we explore the utility of CNDs, with their small size and biointerfacing properties, as a platform for cancer-specific drug delivery (Fig. 1). To achieve this, a modular strategy that allows the rapid generation of different targeted nanoformulations is leveraged [31,32]. Cell membrane is genetically engineered to express SpyCatcher, enabling it to be rapidly and irreversibly modified with any targeting ligand fused to a short SpyTag peptide sequence. Using this membrane, we successfully generate tumor-targeting CNDs loaded with DOX, a model chemotherapeutic. Overall, the formulation exhibits elevated localization to tumors expressing the targeted receptor, resulting in strong antitumor efficacy in a murine breast cancer model.

2. Materials and methods

2.1. Cell culture and protein production

The MDA-MB-231 cell line was acquired from the American Type Culture Collection (CRM-HTB-26) and cultured in Dulbecco's modified Eagle medium (DMEM; Corning) supplemented with 10 % fetal bovine serum (Gibco) and penicillin–streptomycin (Gibco). The SpyCatcher-expressing HEK293 cell line (denoted scCell) was constructed as previously described [31] and cultured in complete DMEM supplemented with 300 μg/mL of hygromycin B (Invivogen).

An affibody targeting epidermal growth factor receptor (EGFR) was genetically fused to the SpyTag003 peptide and subcloned into an expression plasmid as previously described [31]. To produce the resulting ligand (denoted STα), the plasmid was transformed into BL21-CodonPlus (DE3)-RIPL competent cells (Agilent) and plated onto Luria-Bertani (LB) agar (Difco). A single colony was picked and cultured in 1 L of auto-induction media LB broth base including trace elements (Formedium) with 100 μg/mL kanamycin (Sigma-Aldrich) at 30 °C with shaking at 200 rpm. After 24 h, the bacteria were collected, resuspended in a buffer containing 300 mM NaCl (Fisher Scientific), 50 mM Tris–HCl (pH 7.5, Invitrogen), and a protease inhibitor cocktail (Sigma-Aldrich), and lysed using a Fisherbrand Model 120 Sonic Dismembrator. The cell lysate was then centrifuged at 30,000 *g* for 25 min, and the supernatant was collected to purify out the STα via an attached His-tag using

nickel–nitrilotriacetic acid agarose (Qiagen) according to the manufacturer's procedure.

2.2. CND preparation

The cell membrane of scCell (denoted scMem) was derived following a previously described protocol [28]. Briefly, the cells were washed 3 times with a buffer consisting of 225 mM D-mannitol (Sigma-Aldrich), 76 mM sucrose (Sigma-Aldrich), and 30 mM Tris-HCl (pH 7.5, Quality Biological). After being resuspended in the same buffer supplemented with a protease inhibitor cocktail and a phosphatase inhibitor cocktail, the cells were disrupted using a Kinematica Polytron PT 10/35 probe homogenizer at 70 % power for 20 passes. The cell homogenate was then centrifuged at 10,000 *g* for 25 min. The resulting supernatant was collected and centrifuged twice at 150,000 *g* for 35 min using a Beckman Coulter Optima XPN-80 ultracentrifuge. The pellet containing membrane material was resuspended in 0.2 mM ethylenediaminetetraacetic acid (EDTA; Invitrogen) in water and stored at −80 °C for further use.

To prepare affibody-functionalized and drug-loaded CNDs (denoted αND[DOX]), scMem was resuspended in water and incubated with STα at the appropriate weight ratios to form affibody-conjugated membrane (denoted αMem); the final membrane protein concentration was fixed at 1 mg/mL. The mixture was then vortexed at 300 rpm using a Fisher Scientific digital vortex mixer at 4 °C for 1 h. Doxorubicin hydrochloride (DOX; TCI Chemicals) was dissolved in water to create a 10 mg/mL stock solution, which was then added to αMem at a DOX to membrane protein weight ratio of 1:2, and the solution was sonicated for 5 s at 70 % amplitude using a Fisher Scientific 150E Digital Sonic Dismembrator. An equal volume of styrene-maleic acid (SMA; SMALP 200, Cube Biotech) at 50 mg/mL was then added, and the solution was vortexed again at 300 rpm at 4 °C for 16 h. Non-solubilized lipids and proteins were pelleted after ultracentrifugation at 150,000 *g* for 30 min. The CNDs in the supernatant were further purified from free DOX and SMA using Amicon Ultra centrifugal filters (30 kDa MWCO, Millipore Sigma), followed by concentration using these same devices.

CNDs labeled with the fluorescent dye Alexa Fluor 647 (Invitrogen) were prepared following a previously described method [28]. For non-functionalized CNDs with or without DOX (denoted scND[DOX] or scND, respectively), as well as targeted CNDs without DOX (denoted αND), the same process was applied replacing STα and/or DOX with the same volume of buffer.

2.3. Confirmation of affibody conjugation

To determine the dose-dependent conjugation of STα, 1 mg/mL of scMem was mixed with STα at different weight ratios and vortexed at 300 rpm at 4 °C for 1 h. The mixtures were then prepared in NuPAGE LDS sample buffer (Invitrogen). The samples were loaded into a Bolt 4–12 % Bis-Tris 15-well mini protein gel (Invitrogen) and run at 165 V for 45 min in Bolt MOPS SDS running buffer (Invitrogen). Proteins in the gel were then transferred onto a 0.45-μm nitrocellulose membrane (Thermo Scientific) in Bolt transfer buffer (Invitrogen) at 15 V for 30 min. After blocking with 1 % bovine serum albumin (BSA; Sigma-Aldrich) and 5 % nonfat milk (Apex Bioresearch) in phosphate buffered saline (PBS; Corning) containing 0.05 % (*v*/v) Tween 20 (National Scientific), the blots were immunostained with anti-6-His epitope tag (6-His, BioLegend) as the primary stain, followed by horseradish-peroxidase-conjugated anti-mouse IgG (Poly4053, BioLegend) as the secondary stain. Membranes were developed with ECL western blotting substrate (Pierce) and imaged using a Bio-Rad ChemiDoc MP imaging system. Free scMem and STα were used as controls. To evaluate the stability of the conjugation, αMem and αND were incubated in 10 % fetal bovine serum in PBS at 4 °C for 3 days. The samples were then analyzed by western blotting as described above.

2.4. Characterization of CNDs

For size and zeta potential measurements, samples were resuspended in PBS and analyzed using a Malvern Zetasizer Lab Red Label. To assess stability, the nanoparticles were stored at 4 °C, and their sizes were measured every 2 days for a total of 10 days. To visualize morphology, the samples were deposited onto a 400-mesh carbon film grid (Electron Microscopy Sciences), negatively stained with 1 % uranyl acetate (Electron Microscopy Sciences), and then imaged using a JEOL JEM-1400Plus transmission electron microscope. The presence of STα in αMem and αND was confirmed by western blotting as described above. To determine drug encapsulation efficiency, scND[DOX] and αND[DOX] were disrupted in 80 % (*v*/v) dimethyl sulfoxide (DMSO; Fisher Scientific). The fluorescent signal of DOX (excitation/emission = 485/595 nm) was measured using a TECAN Spark 20M microplate multimode reader. To measure the release kinetics of DOX, 200 μL of scND[DOX] or αND[DOX] at a concentration of 1 mg/mL in PBS was added into Slide-A-Lyzer MINI dialysis devices (10 kDa MWCO, Thermo Scientific) and floated on top of 300 mL of PBS at 37 °C. At predetermined timepoints, 10 μL of sample was taken out for fluorescence measurement. Free DOX was used as a control.

2.5. In vitro targeting

For imaging, 3×10^5 MDA-MB-231 cells were seeded overnight into a 30 × 10 mm glass bottom tissue culture-treated dish (CELLTREAT). Dye-labeled scND or αND were added to the dish at a final membrane protein concentration of 5 μg/mL, followed by incubation for 2 h. For blocking, cells were preincubated with STα at a concentration of 1 mg/mL for 2 h. Imaging was performed using a Keyence BZ-X710 fluorescence microscope. For quantitative analysis, cells were seeded into a 24-well tissue culture plate (GenClone) at a density of 1×10^5 per well. After overnight incubation, the cells were collected with 1 mM EDTA in PBS. For affibody blocking, cells were incubated with STα at a concentration of 1 mg/mL for 2 h. Afterwards, the cells were incubated with dye-labeled scND or αND at a membrane concentration of 5 μg/mL for 2 h. Data was collected using a Becton Dickinson LSR-II flow cytometer, and analysis was performed using FlowJo software.

To explore the uptake kinetics of DOX, MDA-MB-231 cells were seeded into a 24-well tissue culture plate at a density of 1×10^5 per well, followed by incubation with free DOX, scND[DOX], and αND[DOX] at a drug concentration of 100 ng/mL. At predetermined timepoints, cells were collected with 1 mM EDTA in PBS, blocked with 1 % BSA in PBS for 30 min at 4 °C, and data was collected using a Becton Dickinson LSR-II flow cytometer. Data analysis was performed using FlowJo software. To visualize uptake, 3×10^5 MDA-MB-231 cells were seeded overnight into a 30 × 10 mm glass bottom tissue culture-treated dish, followed by incubation with free DOX, scND[DOX], and αND[DOX] at a drug concentration of 100 ng/mL for 2 h. The cell nuclei were stained with Hoechst 33342 (Thermo Scientific) for 10 min prior to imaging, which was performed using a Keyence BZ-X710 fluorescence microscope.

2.6. Cytotoxicity assay

To evaluate cytotoxicity, 7.5×10^3 MDA-MB-231 cells were seeded overnight into a 96-well tissue culture plate (GenClone). Cells were then treated with free DOX, scND[DOX], and αND[DOX] at increasing drug concentrations for 4 h, followed by replacement of the medium with fresh complete DMEM. After another 48 h of incubation, cells were washed once with PBS and incubated with 3-[4,5-dimethylthiazol-2-yl]-2,5-diphenyltetrazolium bromide (Sigma-Aldrich) for 1.5 h. Subsequently, the medium was removed, and 100 μL of DMSO was added to dissolve the formazan crystals. The absorbance at 570 nm was measured using a TECAN Spark 20M microplate multimode reader. Untreated cells were used as a 100 % viability control, and those treated with 1 % Triton X-100 (Sigma-Aldrich) were used as a 0 % viability control.

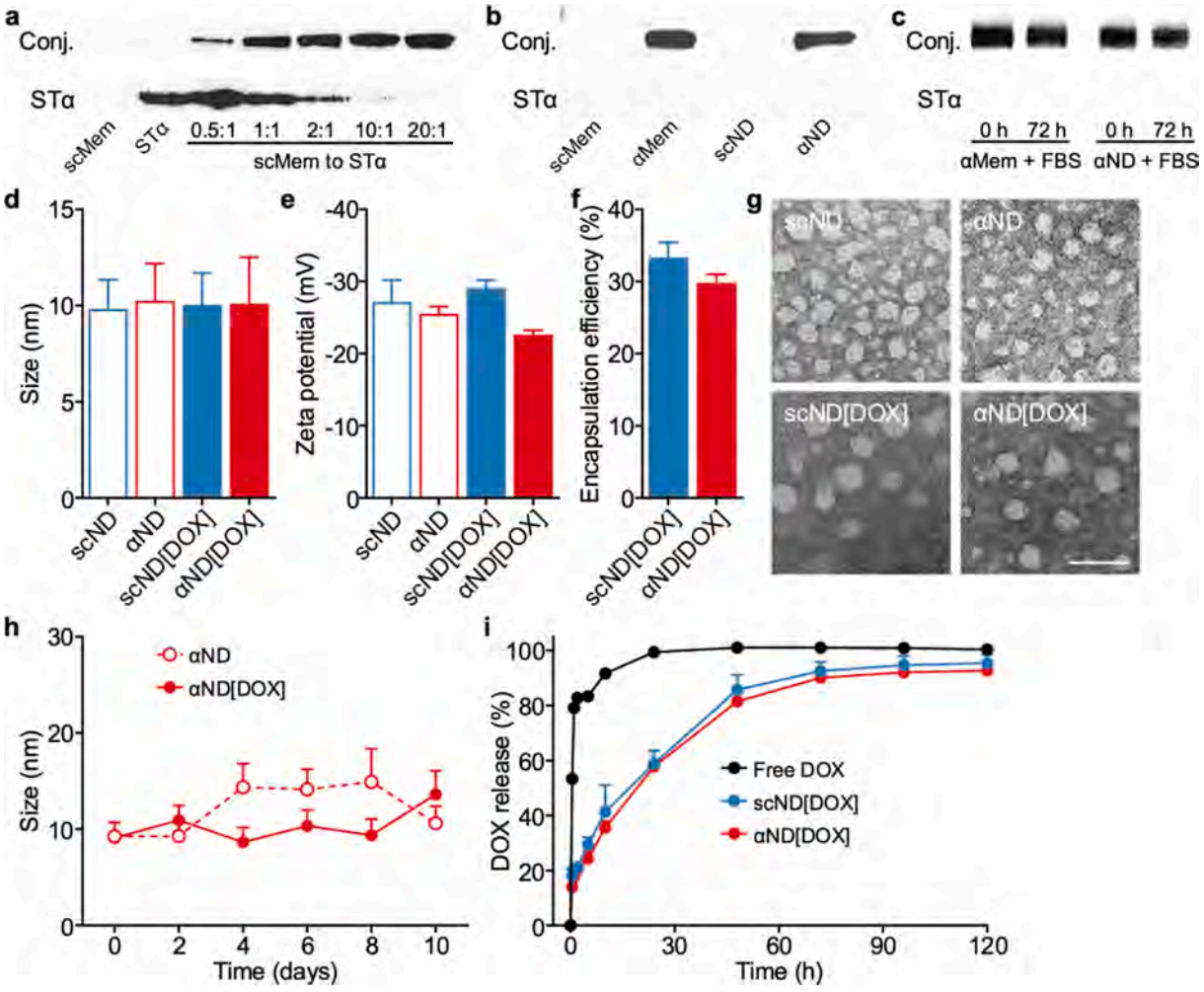

Fig. 2. CND fabrication and characterization. a) Western blot evaluating the conjugation of a SpyTag-labeled anti-EGFR affibody (STα) to SpyCatcher-expressing HEK293 cell membrane (scMem) at different protein weight ratios. Top: conjugate (Conj.), bottom: free STα. b) Western blot probing for the presence of STα on scMem, affibody-functionalized membrane (αMem), nanodiscs fabricated from scMem (scND), and nanodiscs fabricated from αMem (αND). Top: conjugate (Conj.), bottom: free STα. c) Western blot evaluating stability of STα to SpyCatcher conjugation on αMem and αND in fetal bovine serum (FBS) over 72 h. Top: conjugate (Conj.), bottom: free STα. d,e) Size (d) and zeta potential (e) of scND, αND, DOX-loaded scND (scND[DOX]), and DOX-loaded αND (αND[DOX]) ($n = 3$, mean + SD). f) Encapsulation efficiency of DOX in scND[DOX] and αND[DOX] ($n = 3$, mean + SD). g) Transmission electron microscopy images of scND, αND, scND[DOX], and αND[DOX] negatively stained with uranyl acetate. Scale bar = 50 nm. h) Stability of αND and αND[DOX] in 1× phosphate-buffered saline (PBS) at 4 °C ($n = 3$, mean + SD). i) Drug release kinetics for free DOX, scND[DOX], and αND[DOX] ($n = 3$, mean + SD).

2.7. Animal care

Six-week-old male CD1 mice were purchased from Envigo. Six-week-old female nu/nu nude mice were purchased from Charles River Laboratories. All mice were housed in an animal facility at the University of California San Diego (UCSD) under federal, state, and local guidelines. All animal experiments were performed in accordance with National Institutes of Health guidelines and approved by the Institutional Animal Care and Use Committee (IACUC) of UCSD.

2.8. Pharmacokinetics and biodistribution

For the pharmacokinetics study, nu/nu mice were injected with 200 μL of dye-labeled scND and αND at a protein concentration of 0.66 mg/mL. At predetermined timepoints, a drop of blood was collected via submandibular puncture into microtubes coated with sodium heparin (Sigma-Aldrich). Then, 10 μL of each blood sample was diluted with 90 μL of PBS, and the fluorescent signal (excitation/emission = 650/671 nm) of the diluted blood was measured using a TECAN Spark 20M microplate multimode reader. The percentage relative signal was calculated as $(F_t - F_0)/(F_{max} - F_0)$, where F_0 represents the baseline fluorescence in untreated mice, F_t represents the fluorescence at time point t, and F_{max} represents the fluorescence at 1 min. The assay was sensitive enough to detect αND concentrations below 1 μg/mL in blood.

To evaluate tumor targeting and biodistribution, nu/nu mice were inoculated intradermally with 5×10^6 MDA-MB-231 cells in 50 % Matrigel (Corning) on the left flank. Once the average tumor area reached ~70 mm^2, the mice were intravenously injected with 200 μL of dye-labeled scND and αND at a protein concentration of 0.66 mg/mL and imaged using a Xenogen IVIS 200 system at predetermined timepoints. After the final imaging at 24 h, the mice were euthanized, and their main organs and tumors were collected for ex vivo imaging using a Xenogen IVIS 200 system. To quantify the total fluorescence, tissue samples were homogenized with 2-mm zirconia beads (BioSpec) using a BioSpec Mini-BeadBeater-16, and the signals were measured using a TECAN Spark 20M microplate multimode reader.

2.9. Antitumor efficacy study

The tumor model was constructed as described above. Once the

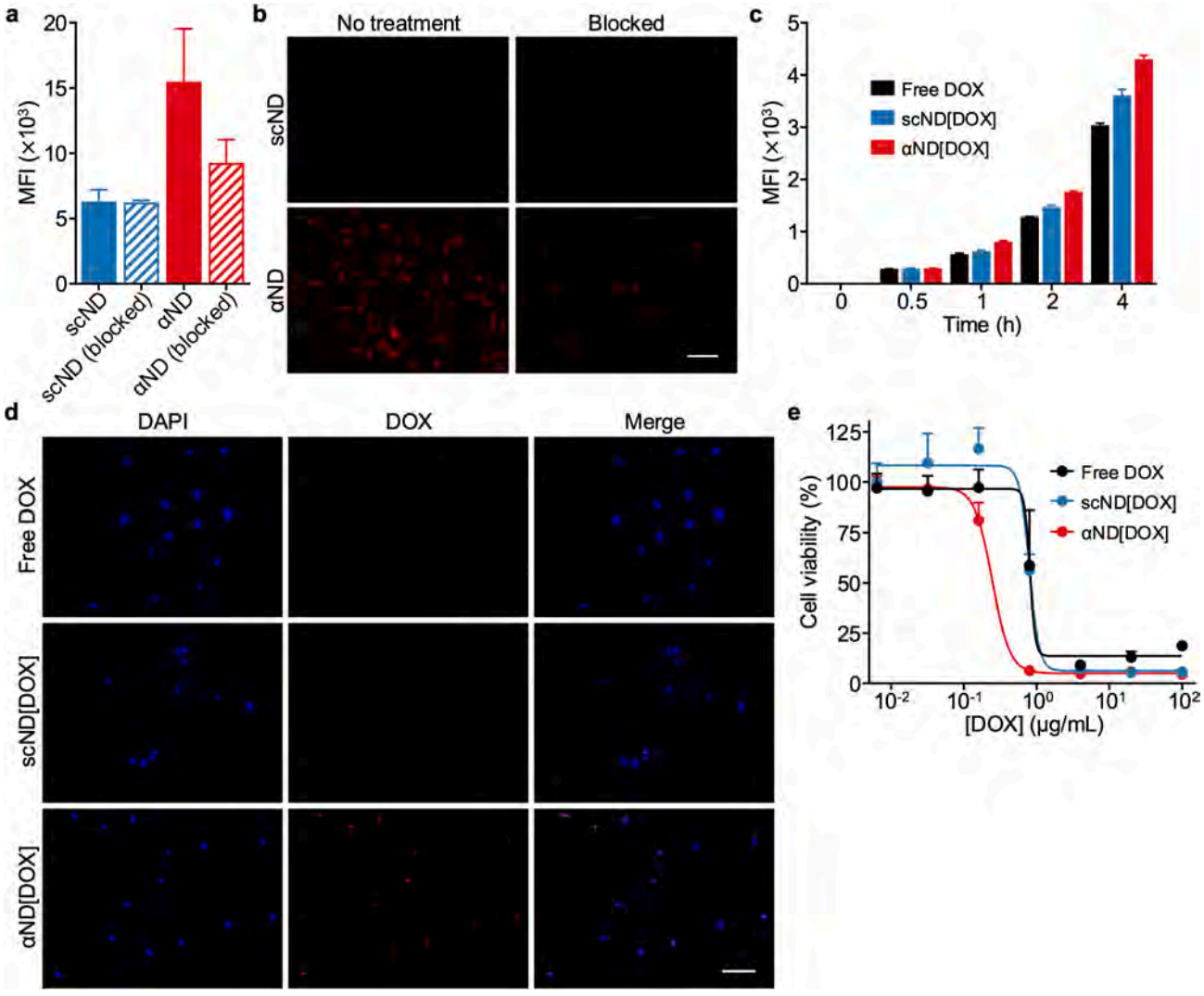

Fig. 3. In vitro characterization. a) Binding of dye-labeled scND and αND after 1 h of incubation with MD-MB-231 cells as measured by flow cytometry ($n = 3$, mean + SD); free STα was used to block specific targeting. b) Representative images visualizing the binding of dye-labeled scND and αND to MD-MB-231 cells after 1 h of incubation; free STα was used to block specific targeting. MFI: mean fluorescence intensity. Red: dye-labeled CND. Scale bar = 50 μm. c) Time-dependent uptake of DOX delivered in free form, scND[DOX], and αND[DOX] by MDA-MB-231 cells ($n = 3$, mean + SD). d) Representative images visualizing DOX uptake after 2 h of incubation in free form, scND[DOX], and αND[DOX]. Blue: nuclei, red: DOX. Scale bar = 50 μm. e) Dose-dependent killing of MDA-MB-231 cells after 4 h of exposure to free DOX, scND[DOX], and αND[DOX], followed by another 48 h of incubation ($n = 6$, mean + SD). (For interpretation of the references to color in this figure legend, the reader is referred to the web version of this article.)

average tumor area reached ~35 mm^2, the mice were intravenously administered with free DOX, scND[DOX], or αND[DOX] at a drug concentration of 2.5 mg/kg via the tail vein every 3 days for a total of 4 injections. Tumor size and body weight were measured every other day. The experimental endpoint was predefined as tumor area > 200 mm^2.

2.10. Biosafety study

CD1 mice were intravenously administered with free DOX, scND[DOX], or αND[DOX] at a drug concentration of 2.5 mg/kg. After 24 h, blood samples were collected via submandibular puncture and allowed to clot, after which the serum was derived by centrifugation at 3000 *g* for 5 min. The samples were then sent to the UCSD Animal Care Program Diagnostic Services Laboratory for complete blood chemistry analysis.

3. Results and discussion

3.1. Preparation of CNDs

To fabricate the modular CNDs, wild-type HEK293 cells were first transduced to express a membrane-bound version of SpyCatcher003, which rapidly forms a covalent bond with the SpyTag003 peptide [33], and the resulting cell line was denoted scCell. An anti-epidermal growth factor receptor (EGFR) affibody was selected as a model targeting ligand and genetically fused with SpyTag. The modified affibody, denoted STα, was expressed in *Escherichia coli* and isolated using nickel–nitrilotriacetic acid affinity chromatography by leveraging its His-tag. Next, the plasma membrane from scCell (denoted scMem) was isolated and incubated with STα to form affibody-functionalized membrane (denoted αMem). The irreversible binding between SpyCatcher and SpyTag was evaluated by incubating scMem with STα at various ratios (Fig. 2a). At a cell membrane to affibody protein weight ratio of approximately 10:1, nearly all STα was bound, and this ratio was selected for further experiments. CNDs were fabricated by incubating either scMem or αMem

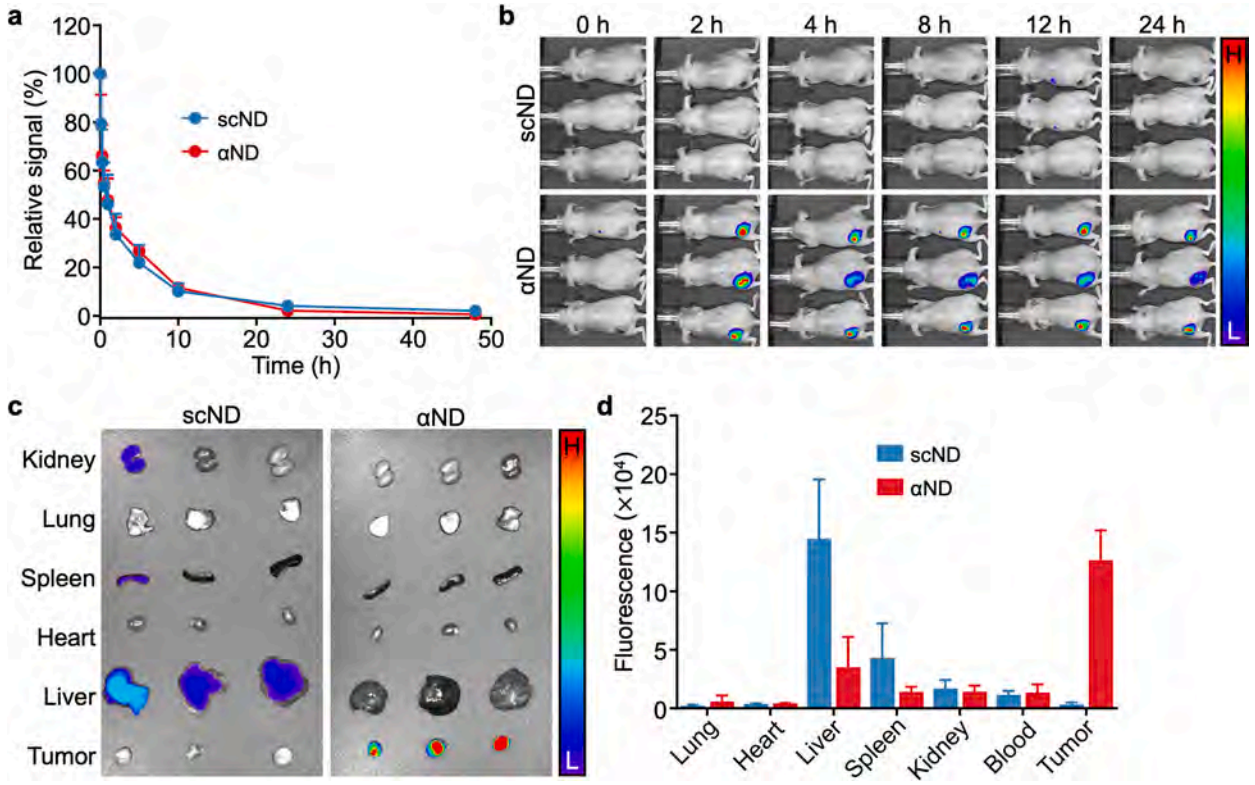

Fig. 4. In vivo characterization. a) Pharmacokinetic profiles of dye-labeled scND and αND after intravenous administration ($n = 3$, mean + SD). b) Live imaging of MDA-MB-231 tumor-bearing nu/nu mice after intravenous administration of dye-labeled scND and αND. H: high signal, L: low signal. c) Ex vivo imaging of organs collected from MDA-MB-231 tumor-bearing nu/nu mice at 24 h after intravenous administration of dye-labeled scND and αND. H: high signal, L: low signal. d) Total fluorescence of organ homogenates from MDA-MB-231 tumor-bearing nu/nu mice at 24 h after intravenous administration of dye-labeled scND and αND ($n = 3$, mean + SD).

with a SMA copolymer as previously described [28]. After fabrication, the successful functionalization of the final targeted CND formulation (denoted αND) was confirmed by western blotting (Fig. 2b). As expected, scNDs fabricated using scMem were not positive for STα. The covalent conjugation of STα to SpyCatcher in αMem and αND remained stable in the presence of serum after 3 days (Fig. 2c). DOX was selected as a model anticancer drug for investigating the potential of αND for nanodelivery. To encapsulate DOX within the final formulation, the drug was premixed with αMem, followed by the addition of SMA. Through the interaction between DOX and the cell membrane, the final drug-loaded and affibody-conjugated CND formulation (denoted αND [DOX]) was successfully formed. As a control, a corresponding non-functionalized drug-loaded formulation (denoted scND[DOX]) was generated.

3.2. Characterization of the CND formulations

The size of all formulations, including scND, αND, and their DOX-loaded counterparts, exhibited near-identical average sizes of approximately 10 nm when measured by dynamic light scattering (Fig. 2d). Their zeta potentials were also within a similar range, from around −22 to −27 mV (Fig. 2e). In terms of encapsulation efficiency, the drug incorporated into scND[DOX] and αND[DOX] equally well at approximately 30 % (Fig. 2f); the main loading mechanism was presumed to be electrostatic in nature. The morphology of both the empty and drug-loaded formulations was visualized using transmission electron microscopy (Fig. 2g). Consistent with previous reports [28], each exhibited a uniform circular shape, indicating that the physical form of the CNDs was minimally affected by the presence of DOX. Furthermore, when stored in 1× PBS solution at 4 °C, the sizes of both αND and αND[DOX] were stable over a period of 10 days (Fig. 2h). Finally, the drug release from scND[DOX] and αND[DOX] was assessed in vitro, and it was revealed that approximately 60 % of DOX was released within 24 h, and approximately 80 % was released within 48 h, after which the kinetics plateaued (Fig. 2i).

3.3. In vitro characterization

To evaluate if affibody conjugation could enhance the targeting ability of the CNDs, MDA-MB-231 cells positive for EGFR [34] were incubated with dye-labeled scNDs or αNDs (Fig. 3a,b). Compared to the scND group, the cells receiving αND showed significantly increased fluorescent signal when analyzing both by flow cytometry and by microscopy. The level of interaction was significantly reduced when the cells were pretreated with free STα as a blocking agent, confirming that the specific targeting ability of αND was mediated by the affibody functionalization. We next evaluated if this enhanced targeting could improve the delivery of a drug payload in vitro. MDA-MB-231 cells were incubated with free DOX, scND[DOX], or αND[DOX], and the level of fluorescent signal from the drug was measured at increasing time intervals by flow cytometry (Fig. 3c). For all samples, there was a time-dependent increase in drug uptake; delivery was the most effective for αND[DOX], with considerable differentiation observed compared with the other groups at 2 h and 4 h. This was corroborated when analyzing by fluorescence microscopy, where cells incubated with αND[DOX] exhibited the strongest signal after 2 h of incubation (Fig. 3d). We further assessed the cytotoxicity of αND[DOX] after incubating with MDA-MB-231 cells for 4 h, followed by replacement with fresh media and incubation for another 48 h (Fig. 3e). Compared to free DOX and scND[DOX], which exhibited IC_{50} values of 0.81 μg/mL and 0.80 μg/mL, respectively, αND[DOX] was more active with an IC_{50} value of 0.25 μg/mL. The data confirmed that, with its enhanced affinity for EGFR, αND

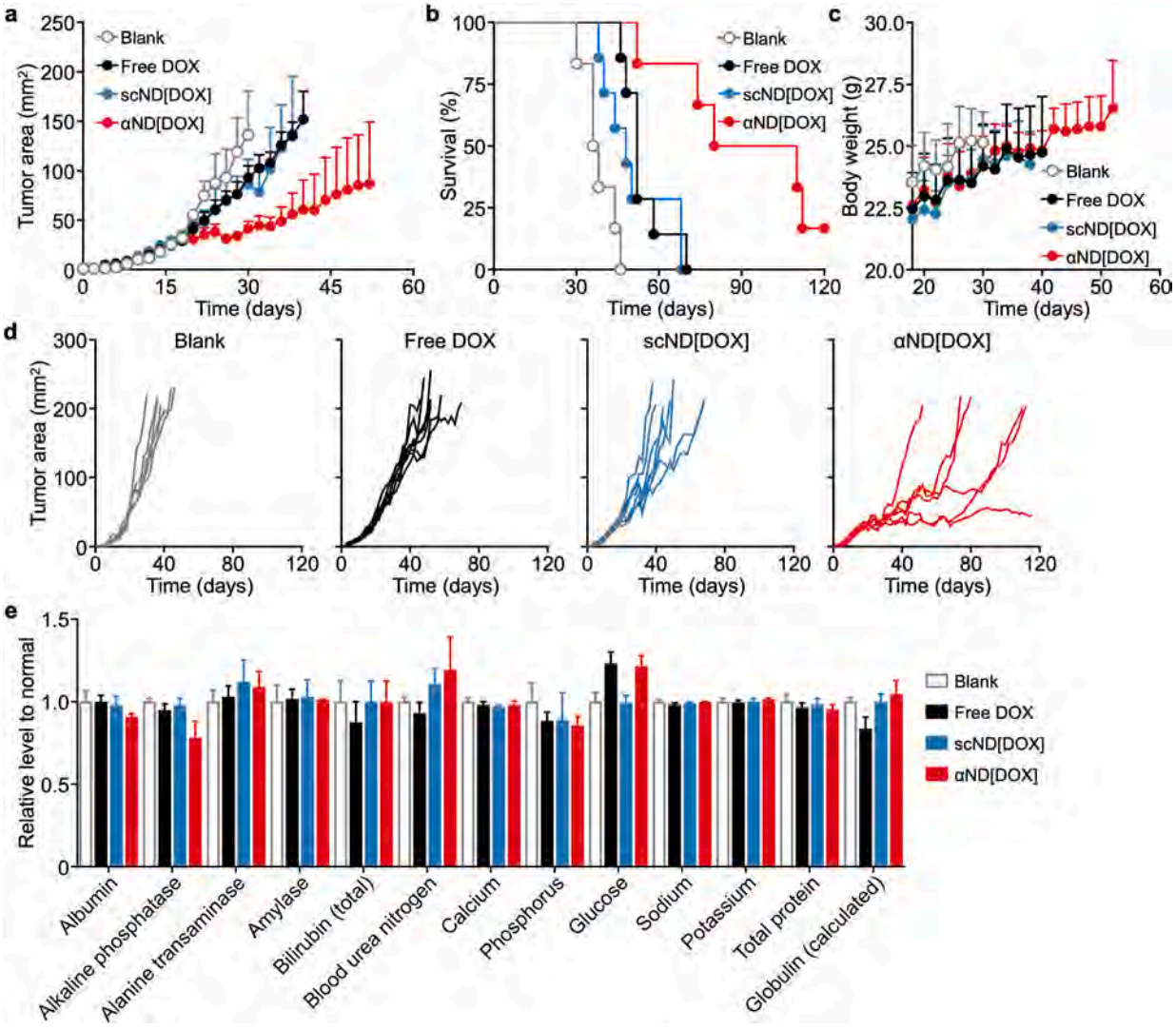

Fig. 5. Therapeutic efficacy and in vivo safety. (a-d) Average tumor size (a), survival (b), body weight (c), and individual tumor kinetics (d) of MDA-MB-231 tumor-bearing nu/nu mice treated with free DOX, scND[DOX], and αND[DOX] every 3 days for a total of 4 treatments after the tumor area reached 35 mm^2 ($n = 6$ for blank and αND[DOX], $n = 7$ for free DOX and scND[DOX], mean + SD). (e) Serum biochemistry of immunocompetent mice at 24 h after receiving free DOX, scND[DOX], and αND[DOX] ($n = 3$, mean + SEM).

was able to better deliver incorporated payloads to improve activity against cancer cells overexpressing the tumor marker.

3.4. *In vivo characterization*

After in vitro characterization of the αND formulation, its in vivo performance was subsequently assessed. To evaluate pharmacokinetics, dye-labeled scND and αND were once again prepared. When administered intravenously, the pharmacokinetic profile of the αND formulation was near-identical its nonfunctionalized counterpart, indicating that the affibody conjugation did not have a pronounced effect on circulation (Fig. 4a). Next, in vivo targeting was evaluated using a murine xenograft tumor model in which MDA-MB-231 cells were intradermally implanted into nude mice. The fluorescent signal of the nanoparticles was visualized over time using in vivo imaging, and significant localization of αNDs at the tumor site was observed as early as 2 h and up to 24 h after intravenous injection (Fig. 4b). In contrast, little to no tumor accumulation was observed for the scND formulation, highlighting the exceptional impact of affibody functionalization on CND targeting and organ distribution. The tumor targeting was further confirmed at 24 h post injection, when the mice were euthanized, and their major organs were imaged ex vivo (Fig. 4c). While most of the signal was associated with the tumors for the αND group, the majority of the signal was found in the liver for scND. Finally, the organs and tumors were homogenized to measure their total fluorescent signal, which further supported the affinity of αND for the $EGFR^+$ tumors (Fig. 4d).

3.5. *Antitumor efficacy and in vivo safety*

As before, a xenograft tumor model was established by intradermal injection of MDA-MB-231 cells into nude mice. When the tumor area reached ~35 mm^2, mice were treated intravenously with free DOX, scND[DOX], or αND[DOX] at a drug dosage of 2.5 mg/kg every three days for a total of four injections (Fig. 5a-d). Compared to untreated mice, both free DOX and scND[DOX] had a moderate impact on tumor growth, prolonging median survival from 37 days to 52 and 48 days, respectively. Treatment with αND[DOX] further slowed the tumor growth kinetics and prolonged survival time to 95 days. In terms of safety, none of the treatments had a significant impact on body weight over the course of the study. Additionally, healthy and immunocompetent CD1 mice were treated with free DOX, scND[DOX], or αND[DOX] at a drug dosage of 2.5 mg/kg. Sera were collected 24 h later for

comprehensive biochemistry analysis (Fig. 5e). Compared to untreated healthy mice, no major differences were observed among the tested parameters for all treatment groups, suggesting good biosafety at the drug dosage that was employed.

4. Conclusions

In conclusion, we have developed a modularly functionalized cellular nanodisc platform capable of delivering chemotherapeutics more specifically to tumor sites. Source cells were modified to express SpyCatcher on their surface, which enabled CNDs fabricated from their plasma membrane to be covalently functionalized with a SpyTag-labeled affibody targeting EGFR. This enabled the resulting affibody-modified CND formulation to exhibit enhanced affinity to cancer cells overexpressing the tumor marker. It was further demonstrated that the nanodiscs could be loaded with a model chemotherapeutic, which improved the drug's cytotoxic activity in vitro against $EGFR^+$ cells. In vivo, the targeted CNDs were better at localizing to tumors versus an untargeted control, allowing for better DOX delivery to inhibit tumor growth in a murine xenograft model. In the future, the applicability of the platform across a broad range of payload types will need to be evaluated. Overall, this work validates the ability of CNDs to be rapidly modified using a modular functionalization approach, which could enable the platform to be generalized to many other targets in the future.

CRediT authorship contribution statement

Ilkoo Noh: Writing – original draft, Investigation, Formal analysis, Conceptualization. **Zhongyuan Guo:** Writing – original draft, Investigation, Formal analysis, Conceptualization. **Rui Wang:** Investigation, Formal analysis. **Audrey T. Zhu:** Methodology, Investigation. **Nishta Krishnan:** Methodology, Investigation. **Animesh Mohapatra:** Investigation. **Weiwei Gao:** Supervision, Resources, Methodology. **Ronnie H. Fang:** Writing – original draft, Supervision, Project administration, Methodology, Funding acquisition, Conceptualization. **Liangfang Zhang:** Writing – review & editing, Supervision, Resources, Methodology, Funding acquisition, Conceptualization.

Declaration of competing interest

The authors declare no conflict of interest.

Acknowledgements

This work was supported by the Defense Threat Reduction Agency Joint Science and Technology Office for Chemical and Biological Defense under award number HDTRA1-21-1-0010 and the National Institutes of Health under Award Number R21AI175904.

Data availability

Data will be made available on request.

References

[1] R.L. Siegel, A.N. Giaquinto, A. Jemal, Cancer statistics, 2024, CA: Cancer, J. Clin. Densitom. 74 (2024) 12–49.
[2] C. Mattiuzzi, G. Lippi, Current cancer epidemiology, J. Epidemiol. Glob. Health 9 (2019) 217–222.
[3] H.Y. Min, H.Y. Lee, Molecular targeted therapy for anticancer treatment, Exp. Mol. Med. 54 (2022) 1670–1694.
[4] A.D. Waldman, J.M. Fritz, M.J. Lenardo, A guide to cancer immunotherapy: from T cell basic science to clinical practice, Nat. Rev. Immunol. 20 (2020) 651–668.
[5] H. Jin, L. Wang, R. Bernards, Rational combinations of targeted cancer therapies: background, advances and challenges, Nat. Rev. Drug Discov. 22 (2023) 213–234.
[6] U. Anand, A. Dey, A.K.S. Chandel, R. Sanyal, A. Mishra, D.K. Pandey, V. De Falco, A. Upadhyay, R. Kandimalla, A. Chaudhary, J.K. Dhanjal, S. Dewanjee, J. Vallamkondu, J.M. Perez de la Lastra, Cancer chemotherapy and beyond: current status, drug candidates, associated risks and progress in targeted therapeutics, Genes Dis. 10 (2023) 1367–1401.
[7] C.M. Tilsed, S.A. Fisher, A.K. Nowak, R.A. Lake, W.J. Lesterhuis, Cancer chemotherapy: insights into cellular and tumor microenvironmental mechanisms of action, Front. Oncol. 12 (2022) 960317.
[8] W.M.C. van den Boogaard, D.S.J. Komninos, W.P. Vermeij, Chemotherapy side-effects: not all DNA damage is equal, Cancers 14 (2022) 627.
[9] K. Bukowski, M. Kciuk, R. Kontek, Mechanisms of multidrug resistance in cancer chemotherapy, Int. J. Mol. Sci. 21 (2020) 3233.
[10] R.J. Browning, P.J.T. Reardon, M. Parhizkar, R.B. Pedley, M. Edirisinghe, J. C. Knowles, E. Stride, Drug delivery strategies for platinum-based chemotherapy, ACS Nano 11 (2017) 8560–8578.
[11] N. Zhao, M.C. Woodle, A.J. Mixson, Advances in delivery systems for doxorubicin, J. Nanomed. Nanotechnol. 9 (2018) 1000519.
[12] G. Wei, Y. Wang, G. Yang, Y. Wang, R. Ju, Recent progress in nanomedicine for enhanced cancer chemotherapy, Theranostics 11 (2021) 6370–6392.
[13] M.I. Khan, M.I. Hossain, M.K. Hossain, M.H.K. Rubel, K.M. Hossain, A. Mahfuz, M. I. Anik, Recent progress in nanostructured smart drug delivery systems for cancer therapy: a review, ACS Appl. Bio Mater. 5 (2022) 971–1012.
[14] A. Kumar, F. Chen, A. Mozhi, X. Zhang, Y. Zhao, X. Xue, Y. Hao, X. Zhang, P. C. Wang, X.J. Liang, Innovative pharmaceutical development based on unique properties of nanoscale delivery formulation, Nanoscale 5 (2013) 8307–8325.
[15] Y. Barenholz, Doxil® — the first FDA-approved nano-drug: lessons learned, J. Control. Release 160 (2012) 117–134.
[16] E. Miele, G.P. Spinelli, E. Miele, F. Tomao, S. Tomao, Albumin-bound formulation of paclitaxel (Abraxane® ABI-007) in the treatment of breast cancer, Int. J. Nanomedicine 4 (2009) 99–105.
[17] R. Bazak, M. Houri, S.E. Achy, W. Hussein, T. Refaat, Passive targeting of nanoparticles to cancer: a comprehensive review of the literature, Mol. Clin. Oncol. 2 (2014) 904–908.
[18] R. Bazak, M. Houri, S. El Achy, S. Kamel, T. Refaat, Cancer active targeting by nanoparticles: a comprehensive review of literature, J. Cancer Res. Clin. Oncol. 141 (2015) 769–784.
[19] N. Kaur, P. Popli, N. Tiwary, R. Swami, Small molecules as cancer targeting ligands: shifting the paradigm, J. Control. Release 355 (2023) 417–433.
[20] P. Gierlich, A.I. Mata, C. Donohoe, R.M.M. Brito, M.O. Senge, L.C. Gomes-da-Silva, Ligand-targeted delivery of photosensitizers for cancer treatment, Molecules 25 (2020) 5317.
[21] C.Y. Beh, R.P. Prajnamitra, L.L. Chen, P.C. Hsieh, Advances in biomimetic nanoparticles for targeted cancer therapy and diagnosis, Molecules 26 (2021) 5052.
[22] C.M.J. Hu, L. Zhang, S. Aryal, C. Cheung, R.H. Fang, L.F. Zhang, Erythrocyte membrane-camouflaged polymeric nanoparticles as a biomimetic delivery platform, Proc. Natl. Acad. Sci. USA 108 (2011) 10980–10985.
[23] R.H. Fang, A.V. Kroll, W. Gao, L. Zhang, Cell membrane coating nanotechnology, Adv. Mater. 30 (2018) 1706759.
[24] Z.Y. Guo, L.J. Kubiatowicz, R.H. Fang, L.F. Zhang, Nanotoxoids: biomimetic nanoparticle vaccines against infections, Adv. Ther. 4 (2021) 2100072.
[25] R.H. Fang, W. Gao, L. Zhang, Targeting drugs to tumours using cell membrane-coated nanoparticles, Nat. Rev. Clin. Oncol. 20 (2023) 33–48.
[26] C.M. Hu, R.H. Fang, K.C. Wang, B.T. Luk, S. Thamphiwatana, D. Dehaini, P. Nguyen, P. Angsantikul, C.H. Wen, A.V. Kroll, C. Carpenter, M. Ramesh, V. Qu, S.H. Patel, J. Zhu, W. Shi, F.M. Hofman, T.C. Chen, W. Gao, K. Zhang, S. Chien, L. Zhang, Nanoparticle biointerfacing by platelet membrane cloaking, Nature 526 (2015) 118–121.
[27] I. Noh, Z. Guo, J. Zhou, W. Gao, R.H. Fang, L. Zhang, Cellular nanodiscs made from bacterial outer membrane as a platform for antibacterial vaccination, ACS Nano 17 (2022) 1120–1127.
[28] Z. Guo, I. Noh, A.T. Zhu, Y. Yu, W. Gao, R.H. Fang, L. Zhang, Cancer cell membrane nanodiscs for antitumor vaccination, Nano Lett. 23 (2023) 7941–7949.
[29] L. Sun, Y. Yu, Y. Peng, D. Wang, S. Wang, I. Noh, R.H. Fang, W. Gao, L. Zhang, Platelet membrane-derived nanodiscs for neutralization of endogenous autoantibodies and exogenous virulence factors, Small 20 (2024) 2308327.
[30] L. Sun, D. Wang, I. Noh, R.H. Fang, W. Gao, L. Zhang, Synthesis of erythrocyte nanodiscs for bacterial toxin neutralization, Angew. Chem. Int. Ed. Eng. 62 (2023) e202301566.
[31] N. Krishnan, Y. Jiang, J. Zhou, A. Mohapatra, F.X. Peng, Y. Duan, M. Holay, S. Chekuri, Z. Guo, W. Gao, R.H. Fang, L. Zhang, A modular approach to enhancing cell membrane-coated nanoparticle functionality using genetic engineering, Nat. Nanotechnol. 19 (2024) 345–353.
[32] B. Zakeri, J.O. Fierer, E. Celik, E.C. Chittock, U. Schwarz-Linek, V.T. Moy, M. Howarth, Peptide tag forming a rapid covalent bond to a protein, through engineering a bacterial adhesin, Proc. Natl. Acad. Sci. USA 109 (2012) E690–E697.
[33] A.H. Keeble, P. Turkki, S. Stokes, I.N.A. Khairil Anuar, R. Rahikainen, V. P. Hytonen, M. Howarth, Approaching infinite affinity through engineering of peptide-protein interaction, Proc. Natl. Acad. Sci. USA 116 (2019) 26523–26533.
[34] B. Corkery, J. Crown, M. Clynes, N. O'Donovan, Epidermal growth factor receptor as a potential therapeutic target in triple-negative breast cancer, Ann. Oncol. 20 (2009) 862–867.